

Constraints on ultralight scalar dark matter from pulsar timing

N.K. Porayko*

Moscow M.V. Lomonosov State University, Faculty of Physics

K.A. Postnov†

*Moscow M.V. Lomonosov State University,
Faculty of Physics, and Sternberg Astronomical Institute*

(Dated: May 12, 2019)

Abstract

We performed a Bayesian analysis of pulsar timing residuals from the NANOGrav pulsar timing array to search for a specific form of stochastic narrow-band signal produced by oscillating gravitational potential in the Galactic halo. Such oscillations arise in models of warm dark matter composed of an ultralight massive scalar field ($m \sim 10^{-23}$ eV), recently considered by Khmelnitsky and Rubakov (2014). In the monochromatic approximation, the stringent upper limit (95% c.l.) on the variable gravitational potential amplitude is found to be $\Psi_c < 1.14 \times 10^{-15}$, corresponding to the characteristic strain $h_c = 2\sqrt{3}\Psi_c < 4 \times 10^{-15}$ at $f = 1.75 \times 10^{-8}$ Hz. In the narrow-band approximation, the upper limit of this background energy density is $\Omega_{\text{GPB}} < 1.27 \times 10^{-9}$ at $f = 6.2 \times 10^{-9}$ Hz. These limits are an order of magnitude higher than the expected signal amplitude. The applied analysis of pulsar timing residuals can be used to search for any narrow-band stochastic signals with different correlation properties. As a by-product, parameters of the red noise present in four NANOGrav pulsars (J1713+0747, J2145-0750, B1855+09, J1744-1134) have been evaluated.

PACS numbers: 04.80.Nn, 95.35.+d, 98.80.-k, 97.60.G

* porayko.nataliya@gmail.com

† pk@sai.msu.ru

I. INTRODUCTION

Gravitational waves (GW), predicted by general relativity (GR), remain major directly non-detected fundamental spacetime features. The indirect evidence for their existence was firmly obtained by measurements of the orbital decay in binary pulsars, which are in agreement with GR to better than half a per cent [1]. Recently, the trace of a primordial stochastic GW background, directly relating to the tensorial nature of GW, was possibly found in the BICEP2 polarization measurements [2], which strongly boosted the interest to GW-astronomy. Prompt development of GW detectors and projects, including ground-based and space interferometers, pulsar timing, measurement of anisotropy of cosmic microwave background, will likely result in the direct detection of GWs in the nearest future (see recent reviews [3]).

Pulsars, which are rapidly rotating neutron stars with highly stable spin frequency, are recognized to be sensitive GW detectors [4]. Especially suitable for GW detection are millisecond pulsars – old neutron stars spun-up to millisecond periods due to accretion in binary systems [5]. A pulsar-timing GW detector is represented by two ‘free’ masses: the Earth and a pulsar. Propagation of a GW induces weak imprint (through the Doppler shift) in the time of arrivals (TOA) of pulses emitted from the pulsar [6]. Potentially, these imprints could be measured by application of statistical methods to the so-called timing residuals (i.e. the difference between the observed and model-predicted TOA). However, TOAs are also influenced by uncertainties in the sky location of the pulsar, model characteristics of the pulsar companion (in the case of binary pulsars [7]), the radio beam propagation effects in through the ionized interstellar medium, etc. The pulsar timing analysis takes into account these model parameters and thus can be used for more accurate determination of physical model of the pulsar itself.

The pulsar timing procedure is sensitive to GW in the frequency range limited by the Nyquist frequency (as determined by the duty cycle of the measurements, about two weeks) and by the whole timespan of the observations (usually several years), i.e. $f_{GW} \in [10^{-9}\text{Hz}; 10^{-7}\text{Hz}]$. In this frequency range, potential astrophysical GW sources include supermassive black hole binaries (SMBHB) [8], which can be located in the centers of galaxies, a stochastic gravitational wave background (GWB) produced by the whole population of SMBHB [9] or, likely, by several bright sources above a weak GWB [10]. The GW detection

procedure is also determined by properties of the sought signal. In the simplest case, in TOA from one pulsar a monochromatic plane GW with amplitude h_c and frequency f produces an oscillatory timing residuals, which also are determined by the pulsar distance D and the relative position of the GW source and the pulsar (via the angle between the direction to the source and the pulsar).

Cross-correlation of residuals from different pulsars can be used to search for stochastic GW signals as well [11]. This concept forms the basis for the construction of Pulsar Timing Arrays (PTA), which nowadays are brought about in EPTA [12], PPTA [13], NANOGrav [14], joint in IPTA [15] (see review of the PTA techniques in [16]). In the last years, the PTA technique resulted in astrophysically interesting upper limits on GW signals of different kinds in the frequency range $10^{-9} - 10^{-7}$ Hz (e.g., [17]).

In addition to the 'traditional' GW sources and stochastic backgrounds that can be probed in the PTA frequency range, there can be more exotic signals, including, for example, GW from oscillating string loops [18], GW signals with memory [19], GW from massive gravitons [20–23]. Recently, Khmelnitsky and Rubakov [24] considered a model of ultralight scalar field with mass $m \sim 10^{-23}$ eV that can be a viable warm dark matter candidate. Different aspects of ultralight scalar fields as warm dark matter have been discussed in the literature, see e.g. [25] and references therein. In the galactic halo, due to huge occupation number, such a field has a coherent part that behaves like a classical wave with amplitude $\sim \sqrt{\rho_{DM}}/m$ and coherence time $\sim 2\pi/(mv^2)$, where $\rho_{DM} \approx 0.3$ GeV/cm³ is the local dark matter density, $v \sim 300$ km/s is the virial halo velocity. As shown in [24], through purely gravitational coupling such a field would produce oscillations of the gravitational potential in the galactic halo at the frequency twice the field mass ($\sim 10^{-8}$ Hz for $m \sim 10^{-23}$ eV), falling within the PTA frequency range. Similar to GW, such oscillations can be sought for in the pulsar timing as monochromatic oscillating residuals with an amplitude corresponding to the characteristic GW strain $h_c \sim 10^{-15}$. Through a dilatonic coupling with the Standard Model particles, these oscillations can also be probed by atomic clock experiments [26].

A distinctive feature of the pulsar timing residuals due to oscillating gravitational potentials produced by variable scalar field is that the amplitude of the TOA residuals should be independent of the pulsar location on the sky. Such a signal is also not a collection of monochromatic GWs with different amplitudes and phases from distant sources. Therefore, it is interesting to put constraints on the amplitude of this specific signal from the available

PTA data, which is the main goal of the present paper. To this aim, we used publically available pulsar timing data from the NANOGrav project, which is described in detail in [27].

The plan of the paper is as follows. In Sec. *II* we introduce the form of the monochromatic signal and correlation matrix for the narrow-band stochastic signal formed by a variable gravitational potential background (GPB). In Sec. *III* we perform the method of data processing based on the likelihood function in the Bayesian approach. In Sec. *IV* we describe the data have been used. In Sec. *V* we summarize our results.

II. SIGNATURES OF A MASSIVE SCALAR FIELD IN PULSAR TIMING

The recent paper [24] considered signatures of a massive scalar field, which can be a viable model for (warm) dark matter, in the pulsar timing observations. The scalar field particles with mass $m \sim 10^{-23}$ eV moving with the galactic virial velocity $v = 10^{-3}$ have a de Broglie wavelength of around 1 kpc, which allows one to describe the galactic halo dark matter in terms of an essentially classical field. The field oscillates with frequency $\approx m$ and can be represented as a collection of almost monochromatic ($\Delta\omega/\omega \sim v^2 \sim 10^{-6}$) plane waves, producing the oscillating pressure and hence, through purely gravitational coupling, the variable gravitational potentials $h_{00} = 2\Phi$ and $h_{ij} = -2\Psi\delta_{ij}$ (in the Newtonian conformal gauge)¹ at frequency $\omega = 2\pi f = 2m$. The propagation of an electromagnetic signal from a pulsar through the time-dependent space-time will leave imprint in the pulsar timing, much like a gravitational wave. From the physical point of view, this is the classical Sachs-Wolfe effect [29]. A derivation for the propagating electromagnetic signal in the special case of time-dependent scalar potentials can be found in the textbook [28] (see Appendix A, where we sketch the derivation of Eq. (3.9) in [24]). The plausible frequency interval of the potential variations in the model considered, $10^{-9} - 10^{-7}$ Hz, can be probed by the current pulsar timing array observations.

Although both scalar potentials Φ and Ψ generally contributes to the redshift of electromagnetic signal propagating from the pulsar to the observer, only the variable part of

¹ Incidentally, we note that in [24], the scalar potential Ψ (their Eq. (2.8)) is initially taken with the minus sign, $h_{ij} = +2\Psi\delta_{ij}$, oppositely to the standard choice [28]. Therefore the sum of the scalar potentials $\Phi + \Psi$ arises in the gradient term in their Eq. (3.2), and not the difference as in the standard literature.

This, however, has no effect for the pulsar timing of interest here.

the potential $\Psi_c \cos(\omega t + \alpha)$ (α is the field phase) can be probed by pulsar timing. It is this part that non-trivially depends on the local dark matter density and the field mass, $\Psi_c \sim \rho_{DM}/m^2$ (see also the discussion below in Section VI).

The form of the resulting signal in the pulsar timing residuals reads [24] (see also Appendix A):

$$R(t) = \frac{\Psi_c}{2\pi f} \{(\sin(2\pi f t + 2\alpha(\mathbf{x}_e)) - \sin(2\pi f(t - D/c) + 2\alpha(\mathbf{x}_p))\}, \quad (1)$$

where f is the frequency, D is the distance to the pulsar, c is the speed of light, $\alpha(\mathbf{x}_e), \alpha(\mathbf{x}_p)$ are the field phase on Earth and at the pulsar, respectively, Ψ_c is the variable potential amplitude to be constrained from PTA timing analysis.

The structure of the timing residuals produced by the variable gravitational potential is reminiscent of that from a plane gravitational wave with amplitude $h_c \sim \Psi_c$, but unlike the GW residuals is independent of the angle between the GW source and the pulsar. Below we will refer to the first and the second term in Eq. (1) as the 'Earth-term' and 'Pulsar-term', respectively.

A. Monochromatic approximation

The expected signal is concentrated within a very narrow frequency band $\delta f/f \sim v^2 \sim 10^{-6}$, much smaller than the current PTA frequency resolution $\Delta f/f \sim 10^{-4}$, and therefore can be treated as monochromatic. Let us examine this case first, i.e. neglect the signal widening due to the final mass of the scalar field particles (see the next Subsection). In this approximation the signal to be searched for in the TOA residuals is given by Eq. (1).

In the PTA technique, given large uncertainties in the pulsar distance estimates, it is common to operate only with Earth terms correlated between different pulsars. For example, the justification for dropping the pulsar term in the case of GW from supermassive black hole binaries is that the pulsar terms add-up at different frequencies and phases [10, 30]. Here we will analyze both cases (including and dropping the pulsar term), as for the GPB produced by the scalar field the Earth and pulsar terms arise in one frequency bin, but still with a phase difference (see also the footnote to Eq. (1) above). Thus, the required signal

forms $s(t)$ can be written as follows:

$$s(t) = R(t) = \begin{cases} \frac{\Psi_c}{2\pi f} \sin(2\pi f t + 2\alpha(\mathbf{x}_e)), & \text{E.termonly} \\ \frac{2\Psi_c}{2\pi f} \sin(\alpha(\mathbf{x}_e) + \frac{\pi f D}{c} - \alpha(\mathbf{x}_p)) \cos(2\pi f t + \alpha(\mathbf{x}_e) + \alpha(\mathbf{x}_p) - \frac{\pi f D}{c}), & \text{E.and P.terms} \end{cases} \quad (2)$$

Below we will denote the effective phase angle due to the pulsar $\theta \equiv \alpha(\mathbf{x}_p) - \pi f D/c$, which is individual for each pulsar and is assumed to be uniformly distributed within the interval $[0, 2\pi]$. A distinguishing feature of such a monochromatic signal is the same amplitude for each pulsar in the array with no connection between their angular positions on the sky.

B. Narrow-band approximation

Now consider the general case of a stochastic narrow-band signal, which is different from the monochromatic case from the point of view of data processing. This approach may be useful in searching for possible narrow-band stochastic signals in PTA data. In addition, in the frame of this approach it is straightforward to relate the amplitude of the oscillating gravitational potential Ψ_c considered in the present paper to the widely used dimensionless power of a stochastic background in the logarithmic frequency interval Ω_{GPB} . We will see that the narrow-band approach gives the same constraints on the signal considered as the monochromatic treatment discussed above, as it should be.

In this approximation, the signal is treated as a narrow-band stationary stochastic background with power contained within the frequency band δf . The properties of this background can be characterized in a way similar to a stochastic GWB, however some difference do arise due to different geometrical structure of GWs and variable gravitational potential signal. To see this difference, it is instructive to start with reminding the standard description of a stochastic GWB [21, 31].

The properties of a stationary statistically homogeneous and isotropic gravitational wave field can be fully described by the metric power spectrum $P_h(k)$ per logarithmic interval of the wavenumber $k = 2\pi f/c$:

$$\langle h_s(k^i) h_{s'}^*(k'^i) \rangle = \delta_{ss'} \delta^3(k^i - k'^i) \frac{P_h(k)}{16\pi k^3} \quad (3)$$

where the angular brackets denote ensemble averaging over all possible realizations, the

mode functions $h_s(k^i)$ correspond to plane monochromatic waves, $s = 1, 2$ correspond to two linear independent modes of polarization.

The dimensionless strain amplitude of the GW field can be defined as:

$$h_c(k)^2 = P_h(k), \quad (4)$$

and the rms amplitude of the GW field is

$$\langle h^2 \rangle = \int P_h(k) d \log k. \quad (5)$$

The characteristic strain h_c fully characterizes the power of the signal. In the case of a narrow-band signal concentrated within some theoretically prescribed interval δk , one may equivalently introduce the spectral amplitude P_0

$$P_h(k') = \begin{cases} P_0, & k < k' < k + \delta k \\ 0, & \text{in other cases,} \end{cases} \quad (6)$$

It can be related to the characteristic strain as

$$h_c^2 = \langle h^2 \rangle = P_0 \delta f / f. \quad (7)$$

However, if the frequency interval determined by the detector resolution $\Delta f \gg \delta f$, only h_c^2 can be probed.

It is also customary to relate the characteristic strain amplitude $h_c(k)$ to the energy density of a stochastic background per logarithmic frequency interval

$$\rho_{\text{GWB}} = (16\pi G)^{-1} 4\pi^2 f^2 h_c^2, \quad (8)$$

or, in dimensionless units,

$$\Omega_{\text{GWB}} = \frac{\rho_{\text{GWB}}}{\rho_{cr}} = \frac{2\pi^2}{3H_0^2} f^2 h_c^2, \quad (9)$$

where the current critical density is $\rho_{cr} = 3H_0^2/(8\pi G)$, H_0 is the present-day Hubble constant.

For the PTA data analysis we will also need the spectrum $S(f)$ of the TOA residuals produced by the sought stochastic signal:

$$\langle R^2 \rangle = \int \frac{dk}{k} P(k) \tilde{R}^2(k) = \int_0^\infty S(f) df. \quad (10)$$

(here $\tilde{R}(k)$ is the transfer function between the GW field and the timing residuals [21]). For example, in the case of an isotropic GWB, the transfer function is $\tilde{R}_{\text{GWB}}^2(k) = 1/(3k^2c^2)$, and for the one-side spectral density of the residuals we obtain the well-known result

$$S_{\text{GWB}}(f) = \frac{h_c^2}{12\pi^2 f^3}, \quad (11)$$

When deriving this formula the averaging over GW tensorial structure and polarization properties has been made. Repeating the derivation of the transfer function $\tilde{R}^2(k)$ as in [21] for the sought signal from oscillating scalar gravitational potential Ψ_c (Eq. (1)), we arrive at

$$S_{\text{GPB}}(f) = \frac{\Psi_c^2}{\pi^2 f^3} \quad (12)$$

which is 12 times as high as Eq. 11. Incidentally, this independently check the relation between the equivalent GW characteristic strain h_c and the amplitude of the varying potential Ψ_c calculate²d in [24] (see their Eq. (3.9)): $h_c = 2\sqrt{3}\Psi_c$. Therefore, in the narrow-band approximation the amplitude Ψ_c can be related to the parameter Ω_{GPB} as follows:

$$\Omega_{\text{GPB}} = \frac{8\pi^2}{H_0^2} f^2 \Psi_c^2. \quad (13)$$

The PTA data analysis requires the knowledge of the covariance function C of the sought signal. For a stochastic background, the variance covariance function C is related to the signal spectral density $S(f)$ via the Wiener-Khinchin theorem:

$$C(\tau) = \int_0^\infty S(f) \cos(\tau f) df. \quad (14)$$

Using the equation for the one-side spectral density Eq. (12) and performing the integration (see APPENDIX C), we obtain the following expression for C_{GPB} :

$$C_{\text{GPB}}(\tau_{ij}) = \zeta_{\alpha\beta} \frac{\Psi_c^2 \delta f}{\pi^2 f^3} \cos(f\tau_{ij}), \quad (15)$$

where $\tau_{ij} = 2\pi|t_i - t_j|$, i, j are indexes of TOA, f is the central frequency of GPB under study. Here $\zeta_{\alpha\beta}$ is the correlation term between pulsars (α, β). As discussed above, GPB oscillations will induce a sinusoidal signal in TOA of each pulsar with the correlation which

² In this expression, the term in the signal redshift containing the integral of spatial gradients of the potentials along the ray is ignored; this term is suppressed by factor $v \sim 10^{-3}$ relative to the value of the potentials, but can be easily taken into account in the PTA data analysis, its contribution being attributed to the field phase uncertainty.

takes the simple form (in contrast, for example, to the case of GWB from merging SMBH binaries):

$$\zeta_{\alpha\beta} = 1/2(1 + \delta_{\alpha\beta}). \quad (16)$$

Here the first and second term arises due to the correlations between the pulsar-term and Earth-term in Eq. (2), respectively.

III. METHOD OF DATA ANALYSIS

Due to the pulsar timing data being not evenly sampled in time and the data containing a time-correlated red noise, we have applied a Bayesian technique developed in [32]. Here we will briefly remind the main points.

Generally, pulsar timing TOA \mathbf{t}^{arr} can be represented by two components: deterministic and stochastic:

$$\mathbf{t}^{arr} = \mathbf{t}^{det}(\boldsymbol{\beta}) + \boldsymbol{\delta t}. \quad (17)$$

The deterministic part is characterized by the pulsar model parameters $\boldsymbol{\beta}$. If the initial guess $\boldsymbol{\beta}_0$ is good, the linear relation between the timing residuals and the uncertainty $\boldsymbol{\zeta} = \boldsymbol{\beta} - \boldsymbol{\beta}_0$ is used.

In our case the random process part $\boldsymbol{\delta t}$ is assumed to include three components: white instrumental noise with a diagonal covariance matrix C_{WN} , a red intrinsic noise characterized by matrix C_{RN} , which could be, for example, due to irregular exchange of momentum between the superfluid component and the crust of the neutron star, and the stochastic background C_{GPB} under study (in the narrow-band approximation). Therefore, the covariance matrix of the random process for TOA of pulsars in the array $\boldsymbol{\delta t}$ includes three components: $C = C_{WN} + C_{RN} + C_{GPB}$ which can be expressed analytically or semi-analytically [33]:

$$C_{WN} = \sigma_{\alpha,i}^2 \delta_{\alpha\beta} \delta_{ij}, \quad (18)$$

$$\begin{aligned} C_{RN} = & \delta_{\alpha\beta} A_{RN,\alpha}^2 \left(\frac{1}{2\sqrt{3}\pi y_{\Gamma}^{-1}} \right)^2 \left(\frac{y_{\Gamma}^{-1}}{f_L} \right)^{\gamma_{RN}^{\alpha}-1} \\ & [\Gamma(1 - \gamma_{RN}^{\alpha}) \sin \frac{\pi \gamma_{RN}^{\alpha}}{2} (f_L \tau_{ij})^{\gamma_{RN}^{\alpha}-1} - \\ & - \sum_{n=0}^{\infty} (-1)^n \frac{(f_L \tau_{ij})^{2n}}{(2n)!(2n+1 - \gamma_{RN}^{\alpha})}], \end{aligned} \quad (19)$$

$$C_{\text{GPB}} = \zeta_{\alpha\beta} \frac{\Psi_c^2 \delta f}{\pi^2 f^3} \cos(f\tau_{ij}), \quad (20)$$

where Γ is the gamma-function. Here A_{RN} , γ_{RN} is the effective strain amplitude and the power-law index of one-sided power spectral density of the red noise, respectively, $\sigma_{\alpha,i}$ is the i -th TOA observation error in data of pulsar α , where $i \in [1, n_\alpha]$, $\alpha \in [1, N]$ (N is the number of pulsars in the array, n_α is the number of observations for pulsar α). The red noise low-frequency cut-off f_L defines the lower limit in the integral (14), providing the convergence for the red-noise indexes $1 < \gamma_{\text{RN}} < 7$.

In the time domain we use a likelihood function in order to estimate the parameters of our model. According to the Bayesian approach, the likelihood function, in the Gaussian approximation, after marginalizing over the unwanted pulsar timing parameters [32] takes the following form:

$$P(\boldsymbol{\delta t}|\boldsymbol{\phi}) = \frac{1}{\sqrt{(2\pi)^{(n-m)} \det(G^T C G)}} \exp\left(-\frac{1}{2} \boldsymbol{\delta t}^T G (G^T C G)^{-1} G^T \boldsymbol{\delta t}\right). \quad (21)$$

Here n is the dimension of $\boldsymbol{\delta t}$, m is a whole number of the unwanted parameters, $\boldsymbol{\phi}$ is the noise parameter vector, G refers to the product of the so-called 'design matrix' that can be obtained using the 'designmatrix' plug-in of the TEMPO2 software [33, 34].

In searching for the deterministic signals (2), we have used the logarithmic likelihood ratio function (the ratio of likelihoods in the case where the signal is present to the case where the signal is absent):

$$\log \Lambda = \boldsymbol{\delta t}^T G (G^T C G)^{-1} G^T \mathbf{s} - 1/2 \mathbf{s}^T G (G^T C G)^{-1} G^T \mathbf{s}, \quad (22)$$

which depends on two parameters: the amplitude Ψ_c and the Earth phase $\alpha(\mathbf{x}_e)$ of the scalar field when using the Earth term only, and on $N + 2$ parameters: the amplitude Ψ_c , the Earth phase $\alpha(\mathbf{x}_e)$ and the phase $\theta_\beta = \alpha(\mathbf{x}_p^\beta) - \pi f D_\beta / c$, if both the Earth and pulsar terms are included. A uniform distribution for $\alpha \in [0; 2\pi]$ and $\theta_\beta \in [0; 2\pi]$ is assumed.

To obtain an upper limit on Ψ_c (Ω_{GPB}) as a function of the central frequency f , we split the entire interesting frequency range into small bins per logarithmic scale ($\delta f / f \simeq 0.03 \ll 1/(5 \text{ yrs})$).

By assuming a uniform trial distribution for f , Ψ_c , Ω_{GPB} and normal trial distribution for γ_{RN} , A_{RN} , we construct a long enough Markov Chain Monte-Carlo (MCMC) [35] for each

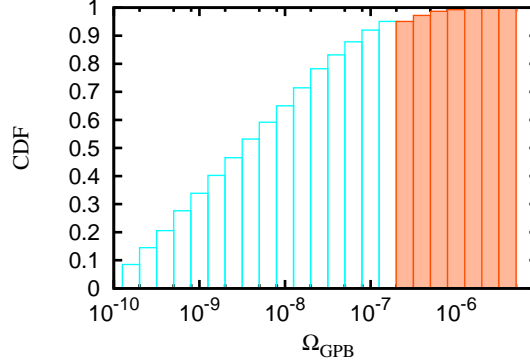


FIG. 1. (Color online). The typical form of the cumulative distribution of Ω_{GPB} in one frequency bin numerically reconstructed by the Monte-Carlo Markov Chain. The blue color (light gray) shows the range containing 95% of all MCMC points. The quantile 0.95 of the Ω_{GPB} CDF gives the 95% confidence level: $\Omega_{\text{GPB}} < \Omega_{0.95}$.

frequency bin. Taking into account the posterior distribution of $\Psi_c(\Omega_{\text{GPB}})$, which is found to be close to a uniform distribution, we can estimate an upper limit as quantile 0.95 of the obtained $\Psi_c(\Omega_{\text{GPB}})$ cumulative distribution (see Fig. 1). In other words, we estimate the posterior distribution of the amplitude with MCMC and assume that the amplitude of the probable signal (even if the signal present) with 95 % probability lies within the $2\text{-}\sigma$ contour [36]. Results of this analysis are presented below in Sec. V.

IV. DATA DESCRIPTION

By applying the method described above, we have processed the real data from the NANOGrav project. The observations, which are in detail described in [37] and are publicly available on ³, were conducted using two radio telescopes, the Arecibo Observatory and the NRAO Green Bank Telescope. Each pulsar was observed nearly 30-60 days during a 5-year period from 2005 to 2010. As the pulsar timing array technique is not sensitive to GWs with 1-day periods, we have conducted the procedure, depicted in [38], to obtain the 'daily averaged' TOA, in order to diminish the signal-to-noise ratio in each observation. The best results were obtained for PSRs J1713+0747 and J1909-3744 with weighted root-mean-square (WRMS) $\sim 20\text{-}30\text{ns}$. The search for a non-white noise component in the NANOGrav data

³ http://www.cv.nrao.edu/~pdemores/nanograv_data/

was performed in [37]. For our purpose, we have chosen the observations of 12 pulsars in one wide frequency band for each pulsar: B1855+09(1400 MHz), J0030+0451(400 MHz), J0613-0200(800 MHz), J1012+5307(800 MHz), J1455-3330(800 MHz), J1600-3053(1400 MHz), J1640+2224(400 MHz), J1713+0747(1400 MHz), J1744-1134(800 MHz), J1909-3744(800 MHz), J1918-0642(800 MHz), J2145-0750(800 MHz). Four of them, J1713+0747, J2145-0750, B1855+09, J1744-1134, show a weak red noise component that should be taken into account (see APPENDIX B). In searches for monochromatic signal we have used only eight white-noise pulsars from the list, since the contamination of the sensitivity occurs due to unmodeled noise sources. In the narrow-band analysis, data for all 12 pulsars from the list were included. The results of the analysis in the monochromatic and the narrow-band approximations were compared using only the eight white-noise pulsars. The post-fit residuals were obtained with the TEMPO2 software [34]. The additive and multiplicative factors (EFAC, EQUAD) were not used in the data pre-processing [39], so these parameters were not added to the 'free parameter' template in our model.

V. RESULTS

In this Section we present the results of searches for GPB produced by massive scalar field oscillations in the NANOGrav pulsar timing data. Working in the time domain we have applied the Bayesian approach developed in [32]. In order to estimate the red noise parameters of pulsars, we have used MCMC to find the distribution of the red noise parameters which were found to be non-Gaussian. In the data analysis we examined three possible signal types: a monochromatic deterministic GPB with the Earth term only, a monochromatic GPB including both the Earth and pulsar terms, and a narrow-band stochastic GPB. In all cases we obtained an upper limit on the signal amplitude Ψ_c (or Ω_{GPB}) as a function of frequency f . The best sensitivity is reached in the case of the monochromatic signal using both Earth and pulsar terms.

In the monochromatic approximation (2), the pulsar timing data is found to be more sensitive when both the Earth and pulsar terms are included, which is likely to be due to the exceeding median value of the amplitude A_{E+P} :

$$\frac{M[A_{E+P}]}{M[A_E]} = \frac{\int 2\cos(\phi)\omega(\phi)d\phi}{1} = \frac{4}{\pi}. \quad (23)$$

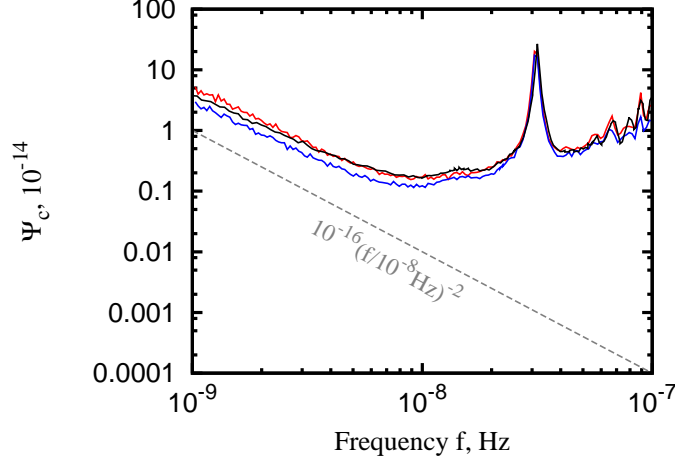


FIG. 2. (Color online). An upper limit on the amplitude of variable gravitational potential Ψ_c due to the massive scalar field oscillations as a function of the central frequency f . Shown is the case of the narrow-band signal approximation (the black line), the monochromatic signal approximation with the Earth term only (the red line), the monochromatic approximation using both the Earth and pulsar terms (the blue line); the lines are shown for the 95% confidence level. Data from 8 pulsars from the NANOGrav project with white-noise rms residuals were used. The dashed line shows the model amplitude (24).

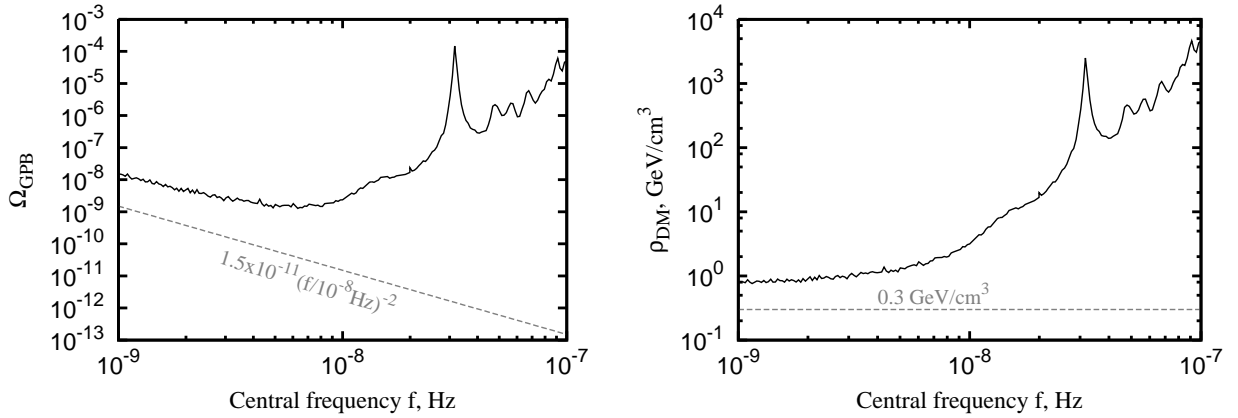


FIG. 3. Left panel: an upper limit on the Ω_{GPB} of the ultralight scalar field as a function of frequency f ; the solid curve corresponds to the 95% confidence level. The dashed line shows the model value (25). Right panel: the same limit in terms of the local dark matter density ρ_{DM} . The dashed line show the local galactic dark matter density 0.3 GeV cm^{-3} . Data from 12 pulsars from the NANOGrav project have been used.

The stringent limit obtained is $\Psi_c < 1.14 \times 10^{-15}$ corresponding to $h_c = 2\sqrt{3}\Psi_c < 4 \times 10^{-15}$ at $f = 1.75 \times 10^{-8}\text{Hz}$ (see Fig. 2).

In the narrow-band approximation the power spectral density of GBP was assumed to have a delta-like form (6). Using a flat prior in the logarithmic scale, we numerically estimated the posterior distribution of the signal power in each frequency bin to set an upper limit on GPB (in terms of Ω_{GPB}). In this case the stringent limit is $\Omega_{\text{GPB}} < 1.27 \times 10^{-9}$ at $f = 6.2 \times 10^{-9}\text{Hz}$, which corresponds to $\Psi_c < 1.5 \times 10^{-15}$ (see Fig. 3).

VI. CONCLUSIONS

The nature of dark matter remains unclear. An ultralight scalar field, which can be possible warm dark matter candidate, produces an oscillating pressure at frequency $\sim m$, which via the gravitational coupling leads to the time-variable gravitational potentials in the galactic halo. For electromagnetic signals propagating through time-dependent space time (the galactic Sachs-Wolfe effect), these oscillations can be treated as a narrow-band stochastic background and thus can be probed in the current pulsar timing data [24], opening new avenues for experimental tests of the possible dark matter candidates.

In the model [24], the dimensionless amplitude of the variable gravitational potential produced by the oscillating massive scalar field Ψ_c is related to the local galactic dark matter density ρ_{DM} and the field mass m as:

$$\Psi_c = \pi \frac{G\rho_{DM}}{(\pi f)^2} \approx 10^{-16} \left(\frac{f}{10^{-8}\text{Hz}} \right)^{-2} \approx 4.3 \times 10^{-16} \left(\frac{m}{10^{-23}\text{eV}} \right)^{-2} \left(\frac{\rho_{DM}}{0.3\text{GeV cm}^{-3}} \right). \quad (24)$$

In terms of the dimensionless energy density of the background (13) we can write:

$$\Omega_{\text{GPB}} \approx 1.5 \times 10^{-11} \left(\frac{f}{10^{-8}\text{Hz}} \right)^{-2} \left(\frac{\rho_{DM}}{0.3\text{GeV cm}^{-3}} \right)^2. \quad (25)$$

The analysis of the NANOGrav PTA data allows us to put constraints on the amplitude of this signal in the monochromatic and narrow-band approximations, which are found to be about one order of magnitude higher than the predicted values (24) and (25). The obtained upper limits (Figs. 2 and 3) are similar in both approximations due to a particularly narrow frequency range of the stochastic signal (less than one frequency bin $\Delta f \sim 1/(5\text{years})$). Still, the narrow-band approach for analysis of pulsar timing residuals as described in Section IIB can be useful in searching for possible stochastic signals with broader spectral width $\delta f/f < 1$.

Therefore, the current PTA data do not constrain the warm dark matter model discussed in [24] in the phenomenologically interesting scalar field mass range $10^{-23} - 2.3 \times 10^{-23}$ eV, corresponding to the gravitational potential oscillation frequency range $\sim (5 - 12)$ nHz. Like in the case of monochromatic and burst GW signals, the sensitivity of PTA technique to the specific stochastic narrow-band GBP produced by oscillating massive scalar field should be determined by the RMS of timing residuals of individual pulsars, unlike broad-band GW backgrounds, sensitivity to which is mostly determined by the number of PTA pulsars [40]. Thus, adding new pulsars with small RMS TOA residuals into the analysis can be crucial to obtain sensitive constraints on the considered model [24] before future projects like SKA [41] become operational.

ACKNOWLEDGMENTS

The authors thank S. Babak, M. Pshirkov, V. Rubakov and the Department of Gravitational Measurements of Sternberg Astronomical Institute for discussions and anonymous referees for useful notes. The use of the publically available NANOGrav PTA data is acknowledged. The work is supported by the Russian Science Foundation grant 14-12-00203.

Appendix A: Photon redshift for Sachs-Wolfe scalar perturbations

As is well known, only tensor perturbations (gravitational waves) cannot freely propagate in free space-time. To better see the difference between the effect of a gravitational wave and variable scalar field in the pulsar timing, it is instructive to remind the reader how the frequency shift appears for a photon propagating in space-time in the presence of variable massive scalar field (the Sachs-Wolfe effect for scalar perturbations). In the covariant Newtonian gauge

$$ds^2 = (1 + 2\Phi(\mathbf{x}, t))dt^2 - (1 - 2\Psi(\mathbf{x}, t))\delta_{ij}dx^i dx^j \quad (\text{A1})$$

the relative frequency shift of a signal emitted at time t' and received at time t'' in linear approximation reads (see [28] for the derivation):

$$\frac{\nu(t'') - \nu(t')}{\nu(t')} = \int_{t'}^{t''} (\partial_t \Phi + \partial_t \Psi) dt + \Phi(t') - \Phi(t''). \quad (\text{A2})$$

Here $c = 1$ and the integral is taking along the unperturbed geodesic $ds^2 = dt^2$. (Note that as in the Newtonian limit Φ plays the role of the Newtonian gravitational potential, in a stationary space-time this formula expresses the standard gravitational redshift of a photon emitted at the point with gravitational potential $\Phi(\mathbf{x}_{em}, t')$ and received at the point with gravitational potential $\Phi(\mathbf{x}_{obs}, t'')$). Changing from partial to full derivative in the first term, $\partial_t = d/dt - n_i \partial_i$, and integrating yields:

$$\frac{\nu(t'') - \nu(t')}{\nu(t')} = \Psi(\mathbf{x}_{obs}, t'') - \Psi(\mathbf{x}_{em}, t') - \int_{t'}^{t''} n_i \partial_i (\Phi + \Psi) dt. \quad (\text{A3})$$

This is Eq.(3.2) in [24]. To see that the second term is small, one can take, for example, expression with changing phase and amplitude and integrate along the trajectory $x = t$:

$$\int_{t'}^{t''} \partial_x (kx(t) \sin(\omega t + kx(t))) dt = \left(-\frac{k\omega}{(\omega + k)^2} \cos(\omega k + t) + \frac{k^2 t}{\omega + k} \sin(\omega k + t) \right) \Big|_{t'}^{t''}. \quad (\text{A4})$$

Even if $k(t'' - t') \sim 1$ and the integrand strongly changes along the trajectory, the result is suppressed by the small factor $k/\omega = v \sim 10^{-3}$ relative to the value of the potentials. It can be easily taken into account in the PTA data analysis, its contribution being attributed to the field phase uncertainty.

Appendix B: Pulsar intrinsic noise

The intrinsic pulsar red noise is a challenging problem in the pulsar timing analysis because it strongly affects the PTA sensitivity to GW signals. The nature of this type of noise is not completely clear and can be related, for example, to irregular momentum exchange between the superfluid component and the crust of the neutron star, as well as with fluctuations of the electron density in the interstellar medium [38]. Therefore, the red noise should definitely be included in the signal model in the data analysis.

The red-noise spectrum is usually assumed to have a power-law form

$$S(f) = \frac{A^2}{12\pi^2} f_0^3 \left(\frac{f}{f_0} \right)^{-\gamma}. \quad (\text{B1})$$

In the time domain, the Wiener-Khinchin theorem allows us to obtain the covariance function presented by Eq. (20). The red noise component characterized by two parameters A_{RN}, γ_{RN} was estimated individually for each of four pulsars (J1713+0747, J2145-0750, B1855+09,

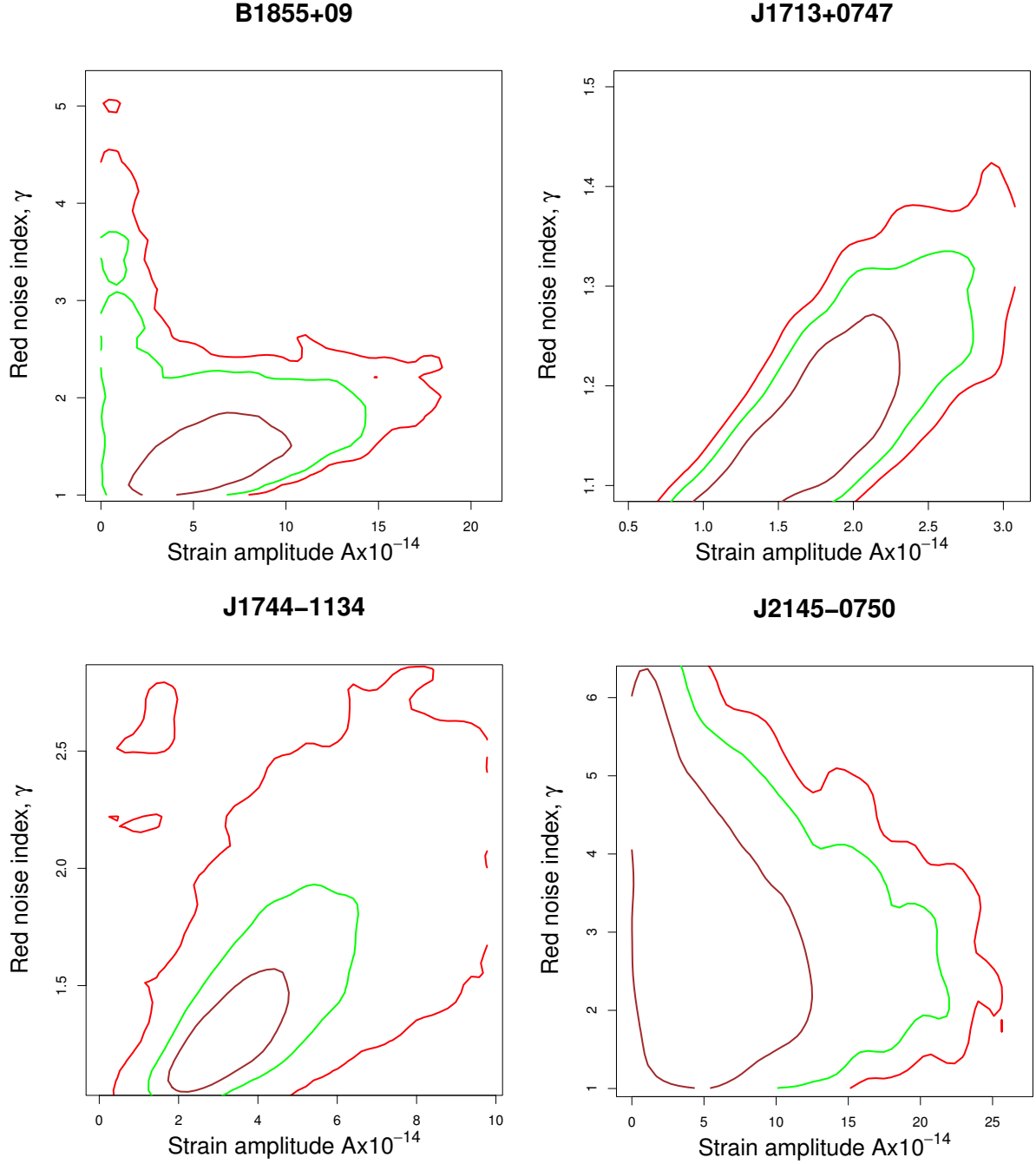


FIG. 4. (Color online). Estimation of the red-noise parameters A_{RN}, γ_{RN} for pulsars J1713+0747, J2145-0750, B1855+09, J1744-1134 using the Markov Chain Monte-Carlo method. Different confident levels are shown in color: brown - 68 % confidence level, green - 95% confidence level, red - 99.7 % confidence level. The plots were obtained using the *R* statistical package ^a.

^a <http://www.r-project.org/>

J1744-1134) by the numerical estimation of the probability distribution from MCMC. The results are presented in Fig. 4. The estimated red-noise parameters for these pulsars have been included in further data analysis to obtain the final results shown in Fig. 3.

Appendix C: Covariance matrix for GPB

The covariance matrix of a stochastic process can be derived from its power spectral density using the Wiener-Khinchin theorem:

$$C(\tau) = \int_0^\infty S(f) \cos(\tau f) df. \quad (\text{C1})$$

In our case, the $S(f)$ has the form (see Eq. 12):

$$S(f) = \frac{Q}{f^3}, \quad (\text{C2})$$

where Q is some constant, therefore the following procedure can be applied. Let us expand $\cos(\tau f)$ in a Maclaurian series:

$$\cos(\tau f) = \sum_{n=0}^{\infty} \frac{(-1)^n}{(2n)!} (\tau f)^{2n}, \quad x \in \mathbb{C}. \quad (\text{C3})$$

After performing the integral, we get:

$$C(\tau) = \sum_{n=0}^{\infty} \frac{(-1)^n}{(2n)!(2n-2)} (\tau)^{2n} f^{2n-2} \left(\left(1 + \frac{\delta f}{f}\right)^{2n-2} - 1 \right). \quad (\text{C4})$$

In the narrow-band approximation $\delta f/f \ll 1$, by expanding $(1 + \frac{\delta f}{f})^{2n-2}$ in a Maclaurin series we find:

$$C(\tau) = \frac{Q}{f^2} \left\{ \cos(f\tau) \left(\frac{\delta f}{f} \right) + (-3 \cos(f\tau) - f\tau \sin(f\tau)) \left(\frac{\delta f}{f} \right)^2 + O \left(\left(\frac{\delta f}{f} \right)^3 \right) \right\}. \quad (\text{C5})$$

A very narrow frequency range of the sought signal allows us to retain only the first-order terms.

[1] C. M. Will, ArXiv e-prints (2014), arXiv:1403.7377 [gr-qc].

- [2] BICEP2 Collaboration, P. A. R. Ade, R. W. Aikin, D. Barkats, S. J. Benton, C. A. Bischoff, J. J. Bock, J. A. Brevik, I. Buder, E. Bullock, C. D. Dowell, L. Duband, J. P. Filippini, S. Fliescher, S. R. Golwala, M. Halpern, M. Hasselfield, S. R. Hildebrandt, G. C. Hilton, V. V. Hristov, K. D. Irwin, K. S. Karkare, J. P. Kaufman, B. G. Keating, S. A. Kernasovskiy, J. M. Kovac, C. L. Kuo, E. M. Leitch, M. Lueker, P. Mason, C. B. Netterfield, H. T. Nguyen, R. O'Brient, R. W. Ogburn, IV, A. Orlando, C. Pryke, C. D. Reintsema, S. Richter, R. Schwarz, C. D. Sheehy, Z. K. Staniszewski, R. V. Sudiwala, G. P. Teply, J. E. Tolan, A. D. Turner, A. G. Vieregg, C. L. Wong, and K. W. Yoon, ArXiv e-prints (2014), arXiv:1403.3985 [astro-ph.CO].
- [3] J. R. Gair, M. Vallisneri, S. L. Larson, and J. G. Baker, Living Reviews in Relativity **16** (2013), 10.12942/lrr-2013-7; N. Yunes and X. Siemens, Living Reviews in Relativity **16** (2013), 10.12942/lrr-2013-9.
- [4] M. V. Sazhin, SvA **22**, 36 (1978); S. Detweiler, ApJ **234**, 1100 (1979).
- [5] D. R. Lorimer, Living Reviews in Relativity **11** (2008), 10.12942/lrr-2008-8.
- [6] F. B. Estabrook and H. D. Wahlquist, General Relativity and Gravitation **6**, 439 (1975).
- [7] S. M. Kopeikin, MNRAS **305**, 563 (1999), physics/9811014.
- [8] F. A. Jenet, G. B. Hobbs, K. J. Lee, and R. N. Manchester, ApJ **625**, L123 (2005), astro-ph/0504458.
- [9] A. Sesana, A. Vecchio, and C. N. Colacino, MNRAS **390**, 192 (2008), arXiv:0804.4476.
- [10] A. Petiteau, S. Babak, A. Sesana, and M. de Araújo, Phys. Rev. D. **87**, 064036 (2013), arXiv:1210.2396 [astro-ph.CO]; S. Babak and A. Sesana, Phys. Rev. D. **85**, 044034 (2012), arXiv:1112.1075 [astro-ph.CO].
- [11] R. W. Hellings and G. S. Downs, ApJ **265**, L39 (1983).
- [12] R. D. Ferdman, R. van Haasteren, C. G. Bassa, M. Burgay, I. Cognard, A. Corongiu, N. D'Amico, G. Desvignes, J. W. T. Hessels, G. H. Janssen, A. Jessner, C. Jordan, R. Karuppusamy, E. F. Keane, M. Kramer, K. Lazaridis, Y. Levin, A. G. Lyne, M. Pilia, A. Possenti, M. Purver, B. Stappers, S. Sanidas, R. Smits, and G. Theureau, Classical and Quantum Gravity **27**, 084014 (2010), arXiv:1003.3405 [astro-ph.HE].
- [13] R. N. Manchester, G. Hobbs, M. Bailes, W. A. Coles, W. van Straten, M. J. Keith, R. M. Shannon, N. D. R. Bhat, A. Brown, S. G. Burke-Spolaor, D. J. Champion, A. Chaudhary, R. T. Edwards, G. Hampson, A. W. Hotan, A. Jameson, F. A. Jenet, M. J. Kesteven,

- J. Khoo, J. Kocz, K. Maciesiak, S. Osowski, V. Ravi, J. R. Reynolds, J. M. Sarkissian, J. P. W. Verbiest, Z. L. Wen, W. E. Wilson, D. Yardley, W. M. Yan, and X. P. You, Publ. Astron. Soc. Australia **30**, e017 (2013), arXiv:1210.6130 [astro-ph.IM].
- [14] M. A. McLaughlin, Classical and Quantum Gravity **30**, 224008 (2013), arXiv:1310.0758 [astro-ph.IM].
- [15] R. N. Manchester and IPTA, Classical and Quantum Gravity **30**, 224010 (2013), arXiv:1309.7392 [astro-ph.IM].
- [16] A. N. Lommen and P. Demorest, Classical and Quantum Gravity **30**, 224001 (2013), arXiv:1309.1767 [astro-ph.IM].
- [17] D. R. B. Yardley, G. B. Hobbs, F. A. Jenet, J. P. W. Verbiest, Z. L. Wen, R. N. Manchester, W. A. Coles, W. van Straten, M. Bailes, N. D. R. Bhat, S. Burke-Spolaor, D. J. Champion, A. W. Hotan, and J. M. Sarkissian, MNRAS **407**, 669 (2010), arXiv:1005.1667 [astro-ph.GA]; Z. Arzoumanian, A. Brazier, S. Burke-Spolaor, S. J. Chamberlin, S. Chatterjee, J. M. Cordes, P. B. Demorest, X. Deng, T. Dolch, J. A. Ellis, R. D. Ferdman, L. S. Finn, N. Garver-Daniels, F. Jenet, G. Jones, V. M. Kaspi, M. Koop, M. Lam, T. J. W. Lazio, A. N. Lommen, D. R. Lorimer, J. Luo, R. S. Lynch, D. R. Madison, M. McLaughlin, S. T. McWilliams, D. J. Nice, N. Palliyaguru, T. T. Pennucci, S. M. Ransom, A. Sesana, X. Siemens, I. H. Stairs, D. R. Stinebring, K. Stovall, J. Swiggum, M. Vallisneri, R. van Haasteren, Y. Wang, and W. W. Zhu, ArXiv e-prints (2014), arXiv:1404.1267.
- [18] T. Damour and A. Vilenkin, Phys. Rev. D. **71**, 063510 (2005), hep-th/0410222.
- [19] M. S. Pshirkov, D. Baskaran, and K. A. Postnov, MNRAS **402**, 417 (2010), arXiv:0909.0742 [astro-ph.CO]; R. van Haasteren and Y. Levin, MNRAS **401**, 2372 (2010), arXiv:0909.0954 [astro-ph.IM].
- [20] S. L. Dubovsky, P. G. Tinyakov, and I. I. Tkachev, Physical Review Letters **94**, 181102 (2005), hep-th/0411158.
- [21] D. Baskaran, A. G. Polnarev, M. S. Pshirkov, and K. A. Postnov, Phys. Rev. D. **78**, 044018 (2008), arXiv:0805.3103.
- [22] M. Pshirkov, A. Tuntsov, and K. A. Postnov, Physical Review Letters **101**, 261101 (2008), arXiv:0805.1519.
- [23] K. Lee, F. A. Jenet, R. H. Price, N. Wex, and M. Kramer, ApJ **722**, 1589 (2010), arXiv:1008.2561 [astro-ph.HE].

- [24] A. Khmelnitsky and V. Rubakov, J. Cosmol. Astropart. Phys. **2**, 019 (2014), arXiv:1309.5888 [astro-ph.CO].
- [25] M. I. Khlopov, B. A. Malomed, and I. B. Zeldovich, MNRAS **215**, 575 (1985); W. Hu, R. Barkana, and A. Gruzinov, Physical Review Letters **85**, 1158 (2000), astro-ph/0003365; A. Arbey, J. Lesgourgues, and P. Salati, Phys. Rev. D. **65**, 083514 (2002), astro-ph/0112324; A. Suárez, V. Robles, and T. Matos, ArXiv e-prints (2013), arXiv:1302.0903 [astro-ph.CO].
- [26] A. Arvanitaki, J. Huang, and K. Van Tilburg, ArXiv e-prints (2014), arXiv:1405.2925 [hep-ph].
- [27] P. B. Demorest, R. D. Ferdman, M. E. Gonzalez, D. Nice, S. Ransom, I. H. Stairs, Z. Arzoumanian, A. Brazier, S. Burke-Spolaor, S. J. Chamberlin, J. M. Cordes, J. Ellis, L. S. Finn, P. Freire, S. Giampanis, F. Jenet, V. M. Kaspi, J. Lazio, A. N. Lommen, M. McLaughlin, N. Palliyaguru, D. Perrodin, R. M. Shannon, X. Siemens, D. Stinebring, J. Swiggum, and W. W. Zhu, ApJ **762**, 94 (2013), arXiv:1201.6641 [astro-ph.CO].
- [28] D. S. Gorbunov and V. A. Rubakov, Introduction to the theory of the early universe (World Scientific Pub. Co., Singapore; Hackensack, N.J., 2011).
- [29] R. K. Sachs and A. M. Wolfe, ApJ **147**, 73 (1967); R. K. Sachs, A. M. Wolfe, G. Ellis, J. Ehlers, and A. Krasinski, General Relativity and Gravitation **39**, 1929 (2007).
- [30] J. A. Ellis, X. Siemens, and J. D. E. Creighton, ApJ **756**, 175 (2012), arXiv:1204.4218 [astro-ph.IM].
- [31] L. P. Grishchuk, V. M. Lipunov, K. A. Postnov, M. E. Prokhorov, and B. S. Sathyaprakash, Physics Uspekhi **44**, 1 (2001), astro-ph/0008481.
- [32] R. van Haasteren and Y. Levin, MNRAS **428**, 1147 (2013), arXiv:1202.5932 [astro-ph.IM].
- [33] R. van Haasteren, Y. Levin, P. McDonald, and T. Lu, MNRAS **395**, 1005 (2009), arXiv:0809.0791.
- [34] G. B. Hobbs, R. T. Edwards, and R. N. Manchester, MNRAS **369**, 655 (2006), astro-ph/0603381.
- [35] M. E. J. Newman and G. T. Barkema, Monte Carlo methods in statistical physics / M.E.J. Newman and G.T. (1999).
- [36] R. van Haasteren, Y. Levin, G. H. Janssen, K. Lazaridis, M. Kramer, B. W. Stappers, G. Desvignes, M. B. Purver, A. G. Lyne, R. D. Ferdman, A. Jessner, I. Cognard, G. Theureau, N. D'Amico, A. Possenti, M. Burgay, A. Corongiu, J. W. T. Hessels, R. Smits, and J. P. W.

- Verbiest, MNRAS **414**, 3117 (2011), arXiv:1103.0576 [astro-ph.CO].
- [37] D. Perrodin, F. Jenet, A. Lommen, L. Finn, P. Demorest, R. Ferdman, M. Gonzalez, D. Nice, S. Ransom, and I. Stairs, ArXiv e-prints (2013), arXiv:1311.3693 [astro-ph.HE].
- [38] A. N. Lommen and P. Demorest, Classical and Quantum Gravity **30**, 224001 (2013), arXiv:1309.1767 [astro-ph.IM].
- [39] R. van Haasteren, Y. Levin, G. H. Janssen, K. Lazaridis, M. Kramer, B. W. Stappers, G. Desvignes, M. B. Purver, A. G. Lyne, R. D. Ferdman, A. Jessner, I. Cognard, G. Theureau, N. D’Amico, A. Possenti, M. Burgay, A. Corongiu, J. W. T. Hessels, R. Smits, and J. P. W. Verbiest, MNRAS **414**, 3117 (2011), arXiv:1103.0576 [astro-ph.CO].
- [40] X. Siemens, J. Ellis, F. Jenet, and J. D. Romano, Classical and Quantum Gravity **30**, 224015 (2013), arXiv:1305.3196 [astro-ph.IM].
- [41] A. Sesana and A. Vecchio, Classical and Quantum Gravity **27**, 084016 (2010), arXiv:1001.3161 [astro-ph.CO].